1   **On the Holocene Evolution of the Ayeyawady Megadelta**

3   Authors:

5   Liviu Giosan[1], Thet Naing[2], Myo Min Tun[3], Peter D. Clift[4], Florin Filip[5],
6   Stefan Constantinescu[6], Nitesh Khonde[1,7], Jerzy Blusztajn[1], Jan-Pieter Buylaert[8],
7   Thomas Stevens[9], Swe Thwin[10]

9   Affiliations:

11   [1]Geology & Geophysics, Woods Hole Oceanographic, Woods Hole, USA
12   [2]Pathein University, Pathein, Myanmar
13   [3]University of Mandalay, Mandalay, Myanmar
14   [4]Geology & Geophysics, Louisiana State University, USA
15   [5]The Institute for Fluvial and Marine Systems, Bucharest, Romania
16   [6]Geography Department, Bucharest University, Bucharest, Romania
17   [7]Birbal Sahni Institute of Palaeosciences, Lucknow, India
18   [8]Technical University of Denmark, Roskilde, Denmark
19   [9]Uppsala University, Uppsala, Sweden
20   [10]Mawlamyine University, Mawlamyine, Myanmar

26   Correspondence to: L. Giosan (lgiosan@whoi.edu)

28
29
30
31
32
33
34
35

36   *submitted to *Earth Surface Dynamics*

37

38   Abstract:

39

40   The Ayeyawady delta is the last Asian megadelta whose evolution has remained
41   essentially unexplored so far. Unlike most other deltas across the world, the Ayeyawady
42   has not yet been affected by dam construction providing a unique view on largely natural
43   deltaic processes benefiting from abundant sediment loads affected by tectonics and
44   monsoon hydroclimate. To alleviate the information gap and provide a baseline for future
45   work, here we provide a first model for the Holocene development of this megadelta
46   based on radiocarbon and optically stimulated luminescence-dated trench and drill core
47   sediments collected in 2016 and 2017, together with a re-evaluation of published maps,
48   charts and scientific literature. Altogether, this data indicates that Ayeyawady is a mud-
49   dominated delta with tidal and wave influences. The sediment-rich Ayeyawady River
50   built meander belt alluvial ridges with avulsive characters. A more advanced coast in the
51   western half of delta (i.e., the Pathein lobe) was probably favored by the more western
52   location of the early course of the river. Radiogenic isotopic fingerprinting of the
53   sediment suggest that the Pathein lobe coast does not receive significant sediment from
54   neighboring rivers. However, the eastern region of the delta (i.e., Yangon lobe) is offset
55   inland and extends east into the mudflats of the Sittaung estuary. Wave-built beach ridge
56   construction during the late Holocene, similar to other several deltas across the Indian
57   monsoon domain, suggests a common climatic control on monsoonal delta
58   morphodynamics through variability in discharge, changes in wave climate, or both.
59   Correlation of the delta morphological and stratigraphic architecture information onland
60   with the shelf bathymetry, as well as its tectonic, sedimentary and hydrodynamic
61   characteristics provide insight on the peculiar growth style of the Ayeyawady delta. The
62   offset between the western Pathein lobe and the eastern deltaic coast appears to be driven
63   by tectonic-hydrodynamic feedbacks as the extensionally lowered shelf block of the Gulf
64   of Mottama amplifies tidal currents relative to the western part of the shelf. This situation
65   probably activates a perennial shear front between the two regions that acts as a leaky
66   energy fence. Just as importantly, the strong currents in the Gulf of Mottama act as an
67   offshore-directed tidal pump that help build the deep mid-shelf Mottama clinoform with
68   mixed sediments from Ayeyawady, Sittaung, and Thanlwin rivers. The highly energetic
69   tidal, wind and wave regime of the northern Andaman Sea thus exports most sediment
70   offshore despite the large load of the Ayeyawady river.

71

Introduction

Asian megadeltas (*Woodroffe et al., 2006*) have a long history of human habitation and anthropogenic impact. With large populations, which increasingly congregate in sprawling megacities, these vast low-lying and ecologically-rich regions are under threat from environmental degradation, climate change and sea level rise. The Ayeyawady (formerly known as Irrawaddy or Ayeyarwady) is the least studied of these megadeltas despite its scientific, social and economic importance (*Hedley et al., 2010*). Located in the larger India-Asia collision zone, the Ayeyawady delta (Fig. 1) bears the imprint of uniquely complex tectonic processes in a region of oblique subduction (*Morley et al., 2017*) and is a repository for unusually large sediment yields under an erosion-prone monsoon climate (e.g., *Giosan et al., 2017*). Sediment redistribution within the delta and on the shelf fronting it is affected by strong tides amplified by the geomorphology of the region (*Ramasawamy and Rao, 2014*). In contrast to other Asian megadeltas, the Ayeyawady river basin is arguably less transformed by post-World War II anthropogenic impacts, although humans have probably affected delta development since at least the Iron Age as agriculture expanded along the river (*Moore, 2007*) and later intensified during the Pyu (~200 BC to 1050 AD), Bagan (~850 to 1300 AD), and Ava (~1350 to 1550 AD) periods. Recent rapid development trends and population growth underline the need to understand the history and document the current state of the Ayeyawady delta.

Although the Ayeyawady River is less regulated compared to other large rivers, plans are afoot to construct several dams across it and this may change the water and sediment regimes, as well as fluxes reaching its low-lying delta plain (*Brakenridge et al., 2017*). Inundation of the Ayeyawady delta region during cyclone Nargis in 2008 was one of the costliest and deadliest natural disasters ever recorded (*Fritz et al., 2009; Seekins, 2009*). Catastrophic monsoon-driven river floods are also common and devastating (*Brakenridge et al., 2017*). The Ayeyawady delta may already be sediment deficient (*Hedley et al., 2010*) and the anticipated sediment deficit after damming could increase its vulnerability to such transient events as well as to long term sea level rise (*Giosan et al., 2014*). Strong tidal currents in the northern Andaman Sea (*Rizal et al., 2012*) amplify some aspects of delta vulnerability, such as salinization (*Taft and Evers, 2016*) whereas other aspects may be attenuated such as sediment redistribution along the coast or sediment trapping within the subaerial delta (e.g., *Hoitink et al., 2017*). Better knowledge on how the delta has formed and functioned will help future efforts to maintain its viability.

To alleviate the information gap and provide a baseline for future work we sketch here a first model for the Holocene evolution of the Ayeyawady delta based on new field data collected in two expeditions in 2016 and 2017 (Figs. 2 and 3; see Fig. S1 for site locations and names) together with a re-evaluation of published maps, charts and scientific literature (Figs. 4 and 5). In the process we reassess our knowledge concerning

113   monsoonal deltas in general by advancing new ideas on how morphodynamics and
114   sedimentary architecture can be controlled by feedbacks between tectonics and tides, as
115   well as by the balance between fluvial discharge and wave climate.
116
117   Background
118
119   The Ayeyawady River is a major fluvial system that became individualized in
120   Oligocene/Early Miocene time (Fig. 1; *Licht et al., 2016; Morley, 2017* and references
121   therein). The Late Cretaceous subduction of the Neotethys Ocean followed by the
122   collision between India and Asia first led to an Andean-type margin comprised of the
123   Wuntho-Popa Volcanic Arc and associated forearc and backarc basins (e.g., *Racey and*
124   *Ridd, 2015; Liu et al., 2016*). The uplift of the Indo-Burman Ranges accretionary prism
125   since early Paleogene completed the separation of the Central Myanmar Basin (CMB)
126   from the Bay of Bengal. The complex of basins forming the CMB were further
127   segmented by compression and inversion (e.g., *Bender, 1983*). These basins include the
128   Ayeyawady Valley separated by the Bago Yoma (Pegu Yoma) from the Sittaung
129   (Sittang) Valley flowing along the Shan Plateau. The Ayeyawady River infilled this ~900
130   km long shallow marine area toward the Andaman Sea, a Cenozoic backarc/strike-slip
131   basin induced by oblique subduction of the Indian plate under Eurasia (e.g., *Curray,*
132   *2005*). A southern shift in Ayeyawady deposition was evident in the Miocene after the
133   major strike-slip fault, the Sagaing, activated along Bago Yoma. The Holocene delta is
134   the last realization in a series of deltas comprising this southward-moving Ayeyawady
135   depocenter.
136
137   Myanmar's hydroclimate that is responsible for Ayeyawady flow is spatially complex
138   owing to its varied topography and compound influences from both the Indian and East
139   Asian monsoon systems (*Brakenridge et al., 2017*). Orographic precipitation occurs
140   along the northeastern Himalayas and Indo-Burman Ranges (*Xie et al., 2006*), as well as
141   the Shan Plateau feeding the upper Ayeyawady and the Chindwin, whereas Central
142   Myanmar, in the lee of these ranges, remains drier. The upper basin of the Ayeyawady
143   also receives snow and glacier meltwater in the spring. Over 90% of the discharge at the
144   delta occurs between May and October with small but significant interannual variability
145   (*Furuichi et al., 2009*) linked to the El Nino-Southern Oscillation, Indian Ocean Dipole,
146   and Pacific Decadal Oscillation (*D'Arigo and Ummenhofer, 2014* and references therein).
147
148   In historical times the Ayeyawady River has transported ~$422 \pm 41 \times 10^9$ m^3 of
149   freshwater every year to the ocean (*Robinson et al, 2007*), watering Myanmar from north
150   to south along the way (Fig. 1). The water discharge has now apparently decreased to the
151   present level of $379 \pm 47 \times 10^9$ m^3/year (*Furuichi et al., 2009*). Among the delta-building
152   Himalayan rivers, the Ayeyawady is a prodigious sediment conveyor (~$364 \pm 60 \times 10^6$

153 t/year), second only to the combined Ganges-Brahmaputra (*Robinson et al, 2007*).
154 Between 40 and 50% of the sediment comes from the upper Ayeyawady, with the rest
155 supplied by its main tributary, the Chindwin (*Garzanti et al., 2016*). Sediments
156 transported by the Upper Ayeyawady River come primarily from erosion of gneisses and
157 granitoids of the Himalayan Eastern Syntaxis region and the Sino-Burman Ranges.
158 Although draining less steep terrain, the Chindwin contributes more sediment than the
159 Upper Ayeyawady from the easily erodible flysch and low-grade metasedimentary rocks
160 of the Indo-Burman Ranges. Both water and sediment discharge vary synchronously at
161 interannual time scales as a function of monsoon intensity (*Furuichi et al., 2009*), but
162 they changed little since the late 19th century when *Gordon (1893)* measured them
163 systematically for the first time. In addition to the Ayeyawady, the Sittaung River
164 supplies sediment to the northern shore of the Gulf of Mottama (*aka* Gulf of Martaban)
165 where its estuary merges with the Ayeyawady delta coast (Fig. 1). The sediment
166 discharge from the Sittaung is unknown but can be estimated based on its annual water
167 discharge range of 50×10^9 m^3/year to a maximum of 40 to 50×10^6 t/year by assuming
168 sediment yields similar to the Ayeyawady (*Milliman and Farnsworth, 2010*). Another
169 sediment contributor to the Gulf of Mottama ($\sim 180 \times 10^6$ t/year) is the Thanlwin River
170 (Salween) draining the eastern Shan Plateau and eastern Tibetan Plateau (*Robinson et al,*
171 *2007*). Information about the variability in Ayeyawady's sediment discharge over the
172 Holocene lifetime of the delta is sparse, as are reconstructions for the monsoon variability
173 in its basin. Assuming the modern direct correlation between water discharge and
174 sediment load one may qualitatively infer an increase in sediment delivery since 10,000
175 years ago with a peak in around 5000 years ago when the Andaman Sea was at its
176 freshest (*Gebregeorgis et al., 2016*), followed by a decrease to the present values, as the
177 Indian monsoon has weakened since the mid Holocene (e.g., *Ponton et al., 2012; Dixit et*
178 *al., 2014*).
179
180 The Ayeyawady delta is a mud-dominated delta that exhibits mainly tidal and secondarily
181 wave influences (Figs. 2 and 5; *Kravtsova et al., 2009*). Ayeyawady's single braided
182 channel starts to show avulsive behaviour near the town of Myan Aung (~18.2°N) where
183 the tidal influence is still felt ~290 km from the Andaman Sea (Fig. 1). The apex of the
184 delta, defined as the region of deltaic distributary bifurcation, is north of the town of
185 Hinthada (18°N) around 270 km from the coast. Multiple branches are active in the delta,
186 splitting and rejoining to form a network of lower order distributary channels and
187 reaching the coast through eleven tidally-enlarged estuaries (Fig. 2). Most of the water
188 discharge (76%) is delivered to the Andaman Sea through three main mouths: Pyamalaw,
189 Ayeyawady and To-Thakutpin from west to east (*Kravtsova et al., 2009*).
190
191 In natural conditions when the delta was covered by tropical forests and mangroves
192 (*Adas, 2011*), sedimentation on the delta plain occurred within active and abandoned

193 channels, on channel levees and inter-distributary basins (*Stamp, 1940; Kravtsova et al.,*
194 *2009*). The coast prograded via shoal/bar emergence and wave-built beach ridges with
195 associated interridge swales (*Kravtsova et al., 2009*). The coastline for the Ayeyawady
196 delta proper stretches from the western rocky Cape Maw Deng, adjacent to the Pathein
197 River, to the Yangon River in the east (Fig. 1). However, this conventional definition
198 does not capture the fact that the accumulative coast with sediment input from the
199 Ayeyawady continues east of the Yangon River into the Sittaung estuary. Despite the
200 large annual fluvial sediment load of the combined Ayeyawady and Sittaung (350–480 ×
201 10^6 t), shoreline changes have been puzzlingly minor along the Ayeyawady delta coast
202 since 1850 (*Hedley et al., 2010*). Sea level change data is sparse and unreliable for the
203 delta and no data on subsidence/uplift exists.
204
205 The shelf morphology in front of the Ayeyawady delta is complex due to its tectonic
206 structure and the nature of Holocene sedimentation (*Rodolfo, 1969a,b, 1975;*
207 *Ramaswamy and Rao, 2014*). The width of the shelf is ~170 km wide off the Ayeyawady
208 River mouths, widening to more than 250 km in the Gulf of Mottama (Figs. 1 and 5). The
209 shelf edge exhibits a flat, platform-like indentation in the Gulf of Mottama between 140
210 and 180 m deep (i.e., the Martaban Depression - *Ramaswamy and Rao,* 2014) that
211 features a dendritic network of channels feeding the Martaban Canyon (*Rodolfo, 1975).*
212 Most of the large Ayeyawady suspended sediment load is redistributed by the strong tidal
213 currents (Fig. 5) and seasonally-reversing wind-currents to be deposited on the wide
214 northern Andaman shelf (*Ramaswamy and Rao, 2014*) where it mixes with sediment
215 from the Sittaung, Thanlwin and other smaller rivers (*Damodararao et al., 2016*). Semi-
216 diurnal tides vary between 2 and 3 m from the Pathein River to the Bogale River,
217 reaching higher stages inside distributaries. The tidal range is gradually amplified to
218 macrotidal conditions on the shallow (<30 m) shelf of the Gulf of Mottama from the
219 Bogale Promontory toward the Sittaung estuary where it reaches above 7 m during spring
220 tides (*British Admiralty, 1935*). Associated tidal currents also vary accordingly to over
221 3.5 m/s near the Sittaung mouth.
222
223 Waves are subordinate in importance for sediment transport to tides, with average heights
224 less than 1 m in winter to 1–2 m in summer (*Kravtsova et al., 2009*). Tidal currents
225 combine with the wind-driven circulation that is clockwise during the summer monsoon
226 and reversed during the winter monsoon (*Rizal et al., 2012*). The macrotidal regime
227 maintains turbid conditions year-round with the turbidity front oscillating ~150 km
228 offshore in the Gulf of Mottama in phase with the spring-neap tidal cycle (*Ramaswamy et*
229 *al. 2004*). Annual turbidity levels and suspended sediment distribution are modulated by
230 the monsoonal-driven winds, currents and river discharge (*Ramaswamy et al. 2004;*
231 *Matamin et al, 2015*) with the most extensive and compact turbid waters occurring in the
232 boreal winter. During the summer the turbidity region shrinks to the Gulf of Mottama and

233   nearshore regions where river plumes are active and dispersed eastward. Turbidity
234   profiles show an increase with depth during fair-weather and uniform concentrations
235   during major storms or cyclones (*Ramaswamy et al. 2004; Shi and Wang 2008*). Bottom
236   nepheloid layers and possibly hyperpycnal flows occur in the Gulf of Mottama and flow
237   into the interior of the Andaman Sea as mid-water nepheloid layers (*Ramaswamy et al.,*
238   *2004*).
239
240   The bathymetric characteristics of the shelf and the circulation system favor deposition of
241   finer fluvial sediments in a mudbelt that widens from the western edge of the Ayeyawady
242   coast into the Gulf of Mottama that more or less coincides in extent with the high
243   turbidity region (*Ramaswamy and Rao, 2014*). The outer shelf, including the Martaban
244   Depression, is a zone of low to non-deposition, and exhibits a relict morphology with
245   topographic irregularities that host relict coarse-grained carbonate-rich sediment and
246   fauna with patchy Holocene muds (*Ramaswamy and Rao, 2014*).
247
248   In terms of human impacts on the delta it is important to note that the population of
249   Myanmar increased from 4–5 million in the late 19th century to ~51 million in 2014 with
250   30% residing in the Ayeyawady delta region. This large increase in population led to a
251   rapid rate of deforestation in the basin, but also to destruction of mangroves for
252   agriculture and fuel in the delta (*Taft and Evers, 2016*). An earlier large migration wave
253   to the delta occurred in the latter half of the 19th century when the British colonial
254   authorities cleared much of the delta forests and mangroves for rice agriculture (*Adas,*
255   *2011*). Construction of dikes to protect agricultural lands in the delta began in 1861 and
256   continued aggressively until the 1920s. These dikes are generally of a horseshoe type
257   protecting delta islands in the upstream and sides from floodwaves but recently poldering
258   with diking entire islands was employed. Most channels remain natural with no extensive
259   system of dredged canals. However, all dikes limit overbank flooding and deposition of
260   sediment (*Volker 1966; Stamp 1940*) and the entire agricultural system favors salinization
261   of soils in the delta. The model for the Holocene evolution of the Ayeyawady delta that
262   we provide below allows us to assess first order relationships to the complex regional
263   tectonics, climate, and shelf circulation as a baseline for the future development and
264   management of the delta.
265
266   Methods
267
268   The large scale morphology of the Ayeyawady delta, together with the adjoining regions
269   (Fig. 2), were assessed and studied using satellite data and old maps of the region. High-
270   resolution (90-m) digital elevation data were derived from NASA's Shuttle Radar
271   Topography Mission (SRTM; *Farr et al., 2007*). Digital elevation models (DEMs) were
272   constructed at 300 m resolution and were used in combination with Advanced
273   Spaceborne Thermal Emission and Reflection Radiometer (ASTER) and Google Earth to

274   identify geomorphic features that provide insight into fluvial morphodynamics. The delta
275   and upstream floodplain was delimited from adjacent hinterlands with associated
276   marginal alluvial fans, as were remnant inselberg-like pre-deltaic terrains inside the delta.
277   We identified active and abandoned river courses and delta distributaries and their
278   meander belts. Finally, we identified fossil beach ridges denoting former delta shorelines.
279   Guided by this assessment, in two field expeditions in the Ayeyawady delta in 2016 and
280   2017, we collected sedimentary records from shallow hand-dug trenches and cores with
281   mechanized pneumatic and percussion drilling (Figs. 2 and 3; see also Fig. S1).
282

283   Fossil wave-built beach ridges were targeted by trenching in order to obtain a chronology
284   for the delta coast advance (Figs. 1 and 2; see also Fig. S1). Samples for Optically
285   Stimulated Luminescence (OSL) dating were collected where possible from within the
286   beach-foreshore facies in water tight opaque tubes (site I-11 at Labutta in the western side
287   of the delta; sites I-12 and I-13 at Seikma near the central delta coast; and site I-14 at
288   Kungyangon near the eastern delta coast). A sample was collected in the anthropogenic
289   overburden to date habitation on a Labutta beach ridge (Site I-10). In addition, two levee
290   samples were collected on meanders of the now defunct western major branch of the
291   Ayeyawady (Figs. 1 and 2; Table 2) near the apex of the delta (i.e., sites I-8 near Ta Loke
292   Htaw and I-9 near Lemyethna bordering the last abandoned course and an earlier-formed
293   oxbow lake, respectively). Levee samples were collected in trenches at the top of each
294   levee, below the overburden.
295

296   Drill coring was designed to recover continuous sediment records to the pre-deltaic
297   Pleistocene sediments (Figs. 2 and 3; see also Fig. S1; Table 1). Drill sites were located
298   in the middle and near the apex of the delta (site IR1 to 70.4 m depth at Kyonmangay
299   located 6.7 m above sea level and core IR2 to 43 m depth at Ta Loke Htaw located at 18
300   m above sea level, respectively) to assess the deltaic architecture and, in particular, how
301   far the post-glacial transgression reached inside the suspected Pleistocene Ayeyawady
302   incised valley. Facies analysis was based on the visual description of lithology,
303   sedimentary structures, textures and benthic foraminifera presence. In addition, XRF-
304   scanning-based high resolution chemostratigraphy was employed for the drill cores to
305   identify depositional environments using Woods Hole Oceanographic Institution's
306   (WHOI) ITRAX XRF scanner (see methodology in *Croudace et al., 2006*). From the
307   suite of measured elements we used [Si]/[Rb] ratio to characterize the sand content (i.e.,
308   Si-rich sand relative to fine grained muds, rich in Rb; *Croudace and Rothwell, 2015*), the
309   [Br]/[total XRF counts] ratio or Br* to characterize the organic matter (i.e., with Br
310   enriched in marine organic matter; *McHugh et al., 2008*), and [S]/[Rb] ratio to
311   characterize redox conditions in fine-grained muds (i.e., with S in excess of terrigenous
312   values in reducing conditions; *Croudace and Rothwell, 2015*).
313

314   Sediment sources for the pre-modern delta were estimated using radiogenic isotopes (Nd
315   and Sr) on a bulk sediment sample from the delta apex trench (I-8 taken as representative
316   for Ayeyawady fluvial sediment). To assess any potential addition of non-Ayeyawady
317   sediment sources (e.g., littoral drift, marine biogenic carbonates) another pre-modern
318   sample from the youngest dated fossil beach ridge trench near the coast (I-12) was
319   measured both as bulk and decarbonated sediment. The radiogenic composition of
320   sediments from the Sittaung River, the closest source to the delta other than Ayeyawady
321   iyself, was measured on a floodplain sample (Fig. ***). Nd and Sr chemistry was
322   undertaken with conventional ion chromatography following the method of *Bayon et al.*
323   *(2002)*. Strontium was separated and purified from samples using Sr-Spec (Eichrom)
324   resin. Nd chemistry was performed with LN resin (Eichrom) following method described
325   in *Scher and Delaney (2010)*. Sr and Nd analyses were conducted on the NEPTUNE
326   multi-collector ICP-MS at WHOI with the internal precision around 10–20 ppm (2σ);
327   external precision, after adjusting $^{87}Sr/^{86}Sr$ and $^{143}Nd/^{144}Nd$ values by 0.710240 and
328   0.511847 for the SRM987 and La Jolla Nd standards respectively, is estimated to be 15–
329   25 ppm (2σ).$^{143}Nd/^{144}Nd$ isotopic composition is expressed further as εNd (*DePaolo and*
330   *Wasserburg, 1976*) units relative to ($^{143}Nd/^{144}Nd$)CHUR= 0.512638 (*Hamilton et al.,*
331   *1983*).
332
333   Plant and wood pieces were radiocarbon-dated to derive a chronology for the deltaic
334   sediment succession and the pre-deltaic base (Table 1). Accelerator mass spectrometry
335   (AMS) radiocarbon dating was performed at the National Ocean Sciences Accelerator
336   Mass Spectrometry Facility (NOSAMS) at the WHOI. The methodology for AMS
337   radiocarbon dating is presented on the NOSAMS site (www.whoi.edu/nosams) and
338   discussed in *McNichol et al. (1995)*. All dates have been converted to calendar ages using
339   CalPal 4.3 (*Bronk Ramsey, 2009*) and the IntCal13 calibration dataset (*Reimer et al.,*
340   *2013*).
341
342   Seven samples were collected for OSL dating. Samples were collected using light-tight
343   metal tubes hammered horizontally into cleaned sediment surfaces. The tubes were
344   opened under subdued orange light at the Nordic Laboratory for Luminescence Dating
345   (Aarhus University) located at Risø (DTU Nutech) in Denmark. Using standard sample
346   preparation techniques (wet sieving, acid treatment, heavy liquids) purified quartz and K-
347   feldspar-rich extracts in the 180–250 μm grain size range were obtained (except sample
348   177202 for which it was 90-180 μm). Multi-grain aliquots of quartz and K-feldspar were
349   measured using a SAR protocol (*Murray and Wintle, 2000*) suitable for young samples.
350   The purity of the quartz OSL signal was confirmed using OSL IR depletion ratio test
351   (*Duller, 2003*; all aliquots within 10% of unity). For quartz OSL preheating for dose and
352   test dose was 200°C/10s and 160°C, respectively and K-feldspar rich extracts were
353   measured using a post-infrared (IR) Infrared Stimulated Luminescence (IRSL)

354 (pIRIR150) protocol based on *Madsen et al.* (2011). Early and late background
355 subtraction was used for quartz OSL and feldspar pIRIR dose calculations respectively.
356 Total dose rates to quartz and K-feldspar were calculated from radionuclide
357 concentrations measured on the outer material from the tubes using high resolution
358 gamma ray spectrometry (*Murray et al., 1987*). Samples were assumed to have been
359 saturated with water throughout the entire burial lifetime.
360
361 The morphology of the subaqueous extension of the Ayeyawady delta was studied using
362 the only available detailed bathymetric chart of the region that was based on surveys from
363 1850 to 1929 with small corrections until 1935 (*British Admiralty, 1935*). Newer
364 navigation charts of the region report only small corrections afterwards. The final DEM
365 (Figs. 4 and 5) consists of 6442 individual soundings reduced to the original datum at
366 Elephant Point at the entrance in Yangon River; to these we added the digitized
367 bathymetric contours of the original chart. To extend the bathymetry offshore beyond the
368 coverage of the original chart we used GEBCO 2014 Grid (General Bathymetric Charts
369 of the Oceans, a global 30 arc-second interval grid). Prior to digitizing, all charts and
370 satellite photos used in this study were georeferenced and transformed to a common
371 UTM projection (Zone 46 N) with Global Mapper 18.0 (http:// www.globalmapper.com/)
372 using 16 control points for each chart or photo. DEMs at a 250 m spatial resolution were
373 generated from digitized soundings with Surfer 12.0 software (Golden Software, Inc.).
374 The ''natural neighbor'' algorithm was chosen for interpolation because it is suitable for
375 a variable density of data across the interpolation domain and does not extrapolate depth
376 values beyond the range of existing data.
377
378 Results
379
380 In concert with satellite photos, our SRTM digital elevation model (Fig. 2a) reveals that
381 the morphologically-defined Ayeyawady delta plain starts immediately after the river
382 emerges from its mountainous valley at Myan Aung, bound on the western side by the
383 Indo-Burma Range and massive alluvial fans originating in the Bago Yoma on the
384 eastern side. Several inselberg-like pre-deltaic high terrains occur close to the coast on
385 the western side of Pathein River and on both sides of Yangon River. Two alluvial ridges,
386 5 to 7 m high relative to their adjacent delta plain, with visible meander belts and rare
387 crevasse splays, were constructed by large trunk channels (Fig. 2a, b, c). The western
388 alluvial ridge along the Daga course is largely fossil, whereas the eastern ridge is being
389 built along the present course of the river (Fig. 2c). Both ridges taper off in the mid-delta
390 as the trunk channels start to bifurcate into distributaries that split and rejoin on the lower
391 delta (Fig. 2a,b). After the bifurcation zone the delta plain is uniformly low in altitude (<5
392 m) with the exception of the higher mudflats near the entrance in the Sittaung estuary
393 (Fig. 2a). Although possessing meander belts of their own in their upper reaches, the
394 Pathein and Yangon Rivers, which are located at the western and eastern edge of the

395 delta, do not show visibly large alluvial ridges (Fig. 2a, b). This suggests that they were
396 not preferential routes for the main trunk Ayeyawady but secondary courses or have not
397 been active for very long. Near the coast, several generations of wave-built beach ridges
398 are evident in the lower part of the delta, bundling occasionally into beach ridge plains on
399 the Bogale Promontory and on the sides on Yangon River (Fig. 2b).
400
401 Sediment in our trenches on the Ayeyawady beach ridges exhibited weakly stratified,
402 mud-rich, fine sand lithologies. Fluvial deposits trenched near the apex showed a typical
403 levee facies exhibiting weakly laminated, amalgamated fine sands and muds below the
404 bioturbated and human-disturbed overburden. The IR1 drill core (Fig. 3) at Kyonmangay
405 (Fig. 2; see also Fig. S1) shows a succession of delta plain bioturbated soils and delta
406 plain muds overlaying amalgamated fine to medium sand and muds of the delta front and
407 prodelta/estuarine clayey muds with intercalated organic-rich detritus layers. Marine
408 influences are documented in the prodelta/estuarine and delta front deposits by high Br*
409 and rare benthic foraminifers. Tidal influence is indicated by thick-thin and sand-mud
410 alternations in the delta front deposits. Flooding is suggested by occasional clean sandy
411 layers in the prodelta facies. Both the delta plain and prodelta/estuarine deposits show
412 increased S/Rb values indicative of poorly oxic conditions. The transition to delta front
413 advance at Kyonmangay occurred at 13.5 m below sea level (mbsl) ~8,100 years ago, as
414 documented by the radiocarbon content of a leaf fragment. The deltaic succession stands
415 on a 9,300 years old mangrove peat at 28.5 mbsl near the base of the deltaic Holocene
416 deposits. Pre-Holocene fluvial deposits older than 10,200 years BP occur below,
417 consisting of structureless medium to coarse sands with clayey mud intercalations,
418 gravels, and fine-grained weakly laminated channel infills.
419
420 The IR2 drill core (Fig. 3) at Ta Loke Htaw (Fig. 2; see also Fig. S1) near the delta apex
421 on the modern alluvial ridge exhibits a succession of delta plain sandy muds topping
422 structureless medium sands with rare intercalated thin muds of channel/point bar type.
423 They overlie fine-grained, weakly laminated channel infill deposits and floodplain fine
424 sands with intercalated thin muds that started to accumulate ~8,900 years BP
425 (radiocarbon dated wood piece). Below ~25 mbsl structureless fine to medium sands of
426 channel/point bar and gravel layers occur to the base of the drill core. Organic material is
427 rare in all facies at Ta Loke Htaw except for occasional wood branches and a tree trunk in
428 the upper point bar facies. Marine influence is absent as foraminifers are not encountered
429 and Br* levels are consistently low.
430
431 The quartz OSL and feldspar pIRIR150 luminescence dating results are summarized in
432 Table 2 and Table S1. The quartz OSL signal is dominated by the fast component and the
433 average dose recovery ratio is 1.00±0.02 (4 samples, 11-12 aliquots per sample)
434 suggesting that our quartz De values measured using SAR are reliable. One prerequisite

435 for accurate age estimation is that the quartz OSL signal was sufficiently bleached prior
436 to burial in the sediment sequence. In this study we use the feldspar IR50 and pIRIR150
437 age data to provide insights into the completeness of bleaching of the quartz OSL signal
438 (e.g., *Murray et al., 2012; Rémillard et al., 2016*). This is based on the observation that
439 feldspar signals bleach much more slowly than quartz OSL (*Godfrey-Smith et al., 1988;*
440 *Thomsen et al., 2008*): IR50 signals bleach approximately one order of magnitude slower
441 than quartz OSL and pIRIR signals bleach even more slowly than IR50 signals (e.g.,
442 *Kars et al., 2014; Colarossi et al., 2015*). We are confident that the quartz signal is well-
443 bleached when the pIRIR150 age agrees within uncertainty with the quartz age; this is the
444 case for sample 177204. We consider that the quartz OSL signal is very likely to be
445 completely bleached when the IR50 age agrees or is slightly lower (due to fading) than
446 the quartz age. This is the case for all samples except for sample 177202 for which the
447 IR50 age may be slightly older. Nevertheless, this does not mean the quartz OSL age for
448 this particular sample is affected by partial bleaching; we just cannot be certain it is not.
449
450 Overall, optical ages on the natural levee of an old meander series of the fossil eastern
451 alluvial ridge indicate full activity by ~1,750±320 years ago. Sedimentation on the top of
452 the natural levee bordering the last Daga course indicates that its abandonment took place
453 no earlier than 1,500±230 years ago (Fig. 2; see also Fig. S1). A radiocarbon date
454 calibrated to ~1,300 years ago on a large wood trunk from the point bar facies drilled at
455 Ta Loke Htaw indicates that the present eastern course of the Ayeyawady was active at
456 the time. The fresh appearance of the wood make it unlikely that it is remobilized fossil
457 wood. Future systematic exploration of the meander belts subsurface architecture is
458 needed to reconstruct their history.
459
460 Our combined chronology indicates the Ayeyawady delta reached as far south as the
461 latitude of the cities of Yangon and Pathein around 6,300 years ago, as documented by a
462 radiocarbon content of a leaf fragment from the delta plain facies at Kyonmangay.
463 Optical dating shows that the least advanced beach ridge bundle found on the western
464 side of the delta near Labutta is also the oldest (~4,600 years old; Fig. 2 and Fig. S1). The
465 beach ridge plain at the Bogale Promontory started ~1,000 years ago, soon after beach
466 ridges started to form at the Yangon River mouth (~1,200 years ago; Fig. 2 and Fig. S1).
467
468 Radiogenic provenance fingerprinting of the bulk river sediment (Table S2) on the Ta
469 Loke Htaw levee shows that $^{143}Nd/^{144}Nd$ (εNd) and $^{87}Sr/^{86}Sr$ values of 0.512263 (-7.3)
470 and 0.7120 respectively, lie close to the beach ridge sediment composition: 0.512285 (-
471 6.9) and 0.7118 for bulk sediment and 0.512287 (-6.8) and 0.7119 for bulk decarbonated
472 sediment. The identical $^{87}Sr/^{86}Sr$ values for the bulk and decarbonated beach ridge sample
473 suggest that marine biogenic carbonates are a minor sediment component at the coast.
474 However, previous measurements on Ayeyawady sediments (Table S2 with data from

475   *Allen et al., 2008* – 150 km upstream of the delta; *Colin et al., 1999* – at an unspecified
476   location) show a larger variability in εNd with values of -8.3 and -10.7. The closest
477   sediment source along the coast, the Sittaung River that drains Bago Yoma and the Shan
478   Plateau shows $^{143}Nd/^{144}Nd$ (εNd) and $^{87}Sr/^{86}Sr$ values of 0.512105 (-10.4) and 0.7168
479   respectively. The Yangon River, the largely abandoned easternmost branch of the
480   Ayeyawady close to Bago Yoma has εNd and $^{87}Sr/^{86}Sr$ of -12.2 and 0.7080 respectively
481   (*Damodararao et al., 2016*), which suggest mixing with a source similar to the Sittaung.
482
483   Our reassessment of the late 19th – early 20th century bathymetry with the high-resolution
484   digital elevation model produced several surprises (Figs. 3 and 4a). First, the edge of the
485   shelf (Fig. 4) was found to be significantly deeper in front of the Mottama Depression
486   (>150 m) than west of it (100–120 m deep). Second, the mud belt along the Ayeyawady
487   delta exhibits a clinoform attached to the shore and likely composed of sandy muds (*Rao*
488   *et al., 2005*) and extending to depths of 35–40 m. In contrast, the Gulf of Mottama
489   exhibits a thick mid-shelf clinoform comprised of finer muds (*Rao et al., 2005*) with the
490   steep frontal region extending from 40 to 90 m water depth. The transition between the
491   western and eastern clinoforms is marked by a transversal channel that is 10 km wide and
492   5 m deep on average and is flanked on the deeper eastern side by a drift-like elongated
493   feature of similar average dimensions. Third, a flatter area of the outer shelf in front of
494   the western Ayeyawady delta coast stands out from the typical outer shelf chaotic relief,
495   suggesting potential preservation of a relict pre-Holocene delta region at water depths
496   between 35 and 45 m.
497
498   Discussion
499
500   Our new drill core information (Fig. 3) indicates that the Holocene Ayeyawady delta
501   advanced into an incised valley estuarine embayment that extended north of
502   Kyonmangay (~80 km from the current coast) but did not reach as far as the current delta
503   apex at Ta Loke Htaw (270 km from the coast). The Pleistocene deposits of the incised
504   valley intercepted in our cores are fluvial, generally much coarser than the delta deposits
505   but heterolithic with indications of increasing tidal influence nearer to the Andaman Sea
506   at Kyonmangay. The overlying peats atop mudflat sediments sampled at Kyonmangay
507   indicate the presence of a muddy coast with mangroves at the time of their transgression
508   ~9,300 years ago. Given that the contemporaneous ice-volume equivalent global sea level
509   was between -29 and -31 mbsl (*Lambeck et al., 2014*), the altitude of the mangrove peat
510   (-28.3 mbsl) on the largely incompressible Pleistocene deposits below indicate that the
511   delta is vertically stable. However, glacial isostatic adjustment modeling is needed to
512   quantify subsidence as neighboring regions of Thailand and Malay Peninsula (*Bradley et*
513   *al., 2016*) suggest that relative sea level reached higher earlier during the deglaciation.
514   After the mangrove coast was flooded, the marine embayment accumulated
515   estuarine/prodelta muds afterwards. At 8,100 years ago the Ayeyawady bayhead delta

516   front reached the southern Kyonmangay site and by ~6,300 years ago delta plain
517   deposition started.
518
519   Deposits at the delta apex in the drill core at Ta Loke Htaw indicate a dynamic fluvial
520   environment with channel erosion (i.e., scouring) followed by point bar and floodplain
521   deposition. The abandonment of the western Daga meander belt after 1,500 years ago,
522   left the Ayeyawady flowing along a single preferential course. Meander belt construction
523   on the old and new course of the river, leading to the formation of alluvial ridges, appears
524   to be an efficient type of aggradation on the upper delta plain before the river starts to
525   bifurcate.
526
527   Near the coast, the quasi-contemporary beach ridge development on the Bogale
528   Promontory and Yangon River mouth argue for the advanced position of the western half
529   of the delta being acquired early and maintained during progradation. Delta growth since
530   6,300 years ago, with intermediate stages delineated by successive beach ridge sets, point
531   to decreasing rates of advance of ~25 m/year until ~4,600 years ago and 8 to 10 m/year
532   afterwards. The latter are still higher than the average progradation value of 3.4 m/year
533   calculated by *Hedley et al. (2010)* for the last century or so. Furthermore, the recent
534   progradation occurred primarily on the coast adjacent to both sides of the Yangon River,
535   while the shoreline of the rest of the delta has been largely immobile. It is important to
536   note that, like the Ayeyawady, many large river deltas developing under the Asian
537   monsoon regime, such as Mekong (*Ta et al., 2002*), Red River (*Tanabe et al., 2003*), or
538   Godavari (*Cui et al., 2017*) started to form wave-built beach ridges between 5000 and
539   4000 years ago changing from river-dominated morphologies to show stronger wave-
540   influenced characteristics. Given that these deltas were at various stages of advance from
541   within their incised valleys onto the shelf it is more likely that their morphological
542   evolution was climatically driven rather than controlled by local factors as previously
543   proposed. As the late Holocene monsoon aridification started at that time (*Ponton et al.,*
544   *2012; Dixit et al., 2014*), fluvial discharge variability at centennial timescales increased
545   setting the stage for periodic wave-dominance of deltaic coasts during more arid
546   intervals.
547
548   Our re-evaluation of the shelf morphology in the context of the new data onland reveals
549   important information for understanding the peculiar, irregular growth of the Ayeyawady
550   delta. Its western half from Cape Maw Deng to the Bogale Promontory is well advanced
551   into the Andaman Sea in comparison to its eastern half. First, the shelf DEM suggests
552   that the western Ayeyawady delta continues offshore into a shallow, coarser-grained
553   shore-attached clinoform, which is not completely unexpected given the relatively low
554   tidal range of 2–3 m (e.g., *Goodbred and Saito, 2012*) and the perennial loss of sediment
555   advected to the Gulf of Mottama (*Ramaswamy and Rao, 2014*). The Nd and Sr

556 fingerprint of the river sediment is almost identical to the beach ridge at Bogale
557 indicating that essentially no sediment from the Gulf of Mottama bearing the radiogenic
558 imprint of Sittaung (see above) and especially Thanlwin (*Damodararao et al., 2016*) is
559 feeding this part of the coast. The shore-attached sandy clinoform tapers off after 40 mbsl
560 (Fig. 2b). In contrast, the Gulf of Mottama exhibits a mid-shelf mud clinoform with the
561 roll-over at 40 m and toe depth of 80–90 m. The internal architecture of this distinctive
562 feature was imaged previously (*Ramaswamy and Rao, 2014*) and showed seismic
563 characteristics typical of a clinoform topset and foreset. High rates of
564 progradation/aggradation for the Mottama clinoform have been suggested previously but
565 a core collected on its lower foreset has an average sedimentation rate of ~1 cm/year
566 since ~1450 AD (Ota et al., 2017), which is one order of magnitude less than proposed
567 before (Chhibber, 1934; Rodolfo, 1975). Given the depressed character of the Mottama
568 shelf, as indicated by the shelf edge position 40 to 70 m lower than in front of the western
569 Ayeyawady delta, perhaps, it is not surprising that infilling of this region is still ongoing.
570 What is surprising instead is why and how the Ayeyawady River built its delta on the
571 eastern raised shelf block rather than in advancing preferentially into the Gulf of
572 Mottama. Such behavior defies theoretical and modeling expectations of a more
573 advanced deltaic coast toward the subsided block (e.g., *Liang et al., 2016*). The key to
574 this problem appears to be again suggested by the shelf morphology.
575
576 The distinctive transition between clinoforms exhibiting a wide elongated channel and
577 what appears to be an attached sediment drift-like feature suggests intense current activity
578 at the common clinoform boundary. Indeed tidal modeling suggests that a tidal shear
579 front (e.g., *Wang et al., 2017*) may be present in this region that shows a drastic change
580 from weak and isotropic tidal currents west of Bogale Promontory to highly oriented
581 strong currents in the Gulf of Mottama (*Rizal et al., 2012*). Such a shear front would
582 explain both the unusual channel-drift couplet, but also the fact the Ayeyawady was able
583 to build its delta west of the gulf. If the tidal shear front has been a long-lived feature of
584 the shelf circulation then it probably acted as a littoral energy fence (*sensu Swift and
585 Thorne, 1992*) trapping a significant part of the Ayeyawady sediment on the raised
586 western shelf block. However, such an energy fence may be broken by prevailing
587 westerly currents during the summer monsoon when water and sediment discharge peaks
588 from the Ayeyarwady to provide finer suspended sediment to the Mottama clinoform.
589 Given the depressed character of the Mottama shelf block, the front must have existed
590 since the beginning of the deglacial transgression of the northern Andaman shelf.
591 Industrial seismic reflection profiles imaged a region of strike-slip extension in the Gulf
592 of Mottama expressed as horsetail extensional splays linked to the Sagaing Fault system
593 (*Morley, 2017*) that can explain the height differential between the western and eastern
594 shelves. Furthermore, the shear front must have gradually intensified through positive
595 feedback with the morphology as the shore-attached clinoform west of it grew larger. In

596 contrast, the amplified tidal currents in the Gulf of Mottama efficiently redistributed the
597 significantly larger amount of Ayeyawady sediments that escaped beyond the energy
598 fence together with sediments from the Sittaung and Thanlwin to form the midshelf
599 clinoform there. The offshore-directed tidal pumping leading to the formation of the
600 Mottama clinoform is reminiscent of the situation on the eastern Indus shelf where strong
601 tidal currents from the Gulf of Kutch built a mid-shelf clinoform with Indus sediments
602 escaping eastward (*Giosan et al., 2006*). Such clinoforms, which are of purely tidal
603 origin, and do not front a subaerial deltaic counterpart *per se* may have been more
604 common in sediment-rich macrotidal environments during faster transgressive conditions
605 in the past.
606
607 Conclusions
608
609 The Ayeyawady delta in Myanmar is the last realization in a long series of depocenters
610 that gradually moved southward within the tectonically dynamic intra-mountainous
611 landscape extending from the Central Myanmar Basin in the north to the northern
612 Andaman Sea in the south (Figs. 1 and 2). The delta developed within the incised valley
613 dug by the Ayeyawady River during the last lowstand (Fig. 3). The Pleistocene valley
614 was flooded at least 80 km inland from the present coast during the deglacial sea level
615 rise. Holocene progradation into this paleo-Ayeyawady bay proceeded in the form of a
616 fluvial- and tide-dominated delta until late Holocene wave action began to build isolated
617 and clustered beach ridges at the contemporaneous coasts (Fig. 2). However, beach ridges
618 are rather rare and underdeveloped, testifying to the enormous sediment load discharged
619 by the Ayeyawady and tidal dispersal and reworking. Ridge construction during the late
620 Holocene, similar to several other deltas across the Indian monsoon domain, argues for a
621 possible climatic control on delta morphodynamics through variability in discharge,
622 changes in wave climate, or both.
623
624 The landscape near the delta apex exhibits active and fossil late Holocene meander belts
625 that terminate in the mid-delta where the discharge is split to lower order distributary
626 channels (Fig. 2). The meander belts stand as alluvial ridges above the floodplain along
627 the active river course, as well as its antecedent paleo-course documenting the
628 Ayeyawady's avulsive character. Construction of a more advanced coast in the western
629 half of the delta could be seen as a quasi-independent region, the Pathein lobe (Fig. 5),
630 which was probably favored by the more western location of the early course of the river
631 (but see below). The eastern region of the delta (the Yangon lobe) is offset inland (Fig. 5)
632 and exhibits a more wave-dominated morphology, largely built with Ayeyawady-derived
633 sediment escaping alongshore. Further east, the Yangon lobe merges with the mudflats
634 fringing the Sittaung estuary (Fig. 5). Despite its large sediment load the Thanlwin River
635 has only built a bayhead delta, barely prograding outside its incised valley, probably due

636   to extreme macrotidal conditions at its mouth (Fig. 5). However, its sediment instead
637   contributed to deposition on the shelf, as did part of the load from both Ayeyawady and
638   Sittaung.

639

640   Correlation of the delta morphological and stratigraphic architecture information onland
641   to the shelf bathymetry and hydrodynamics, as well as its tectonic and sedimentary
642   characteristics, provides insight on the peculiar growth style of the Ayeyawady delta
643   (Figs. 2–5). The offset between the western Pathein lobe and the eastern deltaic coast
644   appears to be driven by tectonic-hydrodynamic feedbacks as the extensionally lowered
645   shelf block of the Gulf of Mottama amplifies tidal currents relative to the eastern part of
646   the shelf. This situation probably activates a perennial shear front between the two
647   regions that behaves as a leaky energy fence. Just as importantly, the strong currents in
648   the Gulf of Mottama act as an offshore-directed tidal pump that help build a deep, mixed-
649   source mid-shelf clinoform, the Ayeyawady-Sittaung-Thanlwin subaqueous delta, into
650   the Mottama shelf depression.

651

652   Our study takes a first look at the evolution of the Holocene Ayeyawady delta to provide
653   a basis for more detailed work and context to present and future management plans for
654   this ecologically and economically important, but vulnerable region. A first conclusion
655   for the future of the region comes by comparing the Ayeyawady to other deltas across the
656   world. Uniquely for deltas of its size the Ayeyawady delta has not suffered a sediment
657   deficit from damming, yet it has been barely growing. The reason is the highly energetic
658   tidal, wind and wave regime of the northern Andaman Sea that exports most sediments
659   offshore despite the large load of the river as envisioned by *Ramswamy et al., (2004)* and
660   *Hedley et al. (2010)*. In addition to their effects upstream (*Brakenridge et al., 2017*), the
661   expected sediment deficit after dams are constructed on the river and tributaries may
662   significantly impact the delta fragile sedimentary equilibrium (*Giosan et al., 2014*). This
663   could make it more vulnerable to the accelerating sea level rise (*Syvitski et al., 2009*) or
664   changes in frequency and intensity of cyclones hitting the coast (*Darby et al., 2016*) that
665   compound with increased subsidence linked to the rapid development of the region (e.g.,
666   Van der Horst, 2017).

667

668

669   Acknowledgments
670
671   We are greatful to reviewers Kelvin Rodolfo and Torbjörn Törnqvist for their
672   suggestions. This study was primarily supported by an Andrew W. Mellon Foundation
673   Award for Innovative Research from the Woods Hole Oceanographic Institution to L.
674   Giosan. Additional funds were provided by the Charles T. McCord Chair in Petroleum
675   Geology to P. Clift. We thank Myanmar authorities for project permissions as well as
676   leaders and residents of villages that we visited in the Ayeyawady delta for hospitality
677   and help. We also thank V. Ramaswamy (NIO, Goa) for providing inspiration with his
678   previous Andaman Sea work and for help with initial contacts in Myanmar. N. Khonde
679   gratefully acknowledges the SERB Indo-US Postdoctoral Fellowship sponsored by
680   SERB-IUSSTF for research work at Woods Hole Oceanographic Institution, USA.
681

682   References
683

684   Allen, R., Najman, Y., Carter, A., Barfod, D., Bickle, M. J., Chapman, H. J., ... & Parrish,
685   R. R. (2008). Provenance of the Tertiary sedimentary rocks of the Indo-Burman
686   Ranges, Burma (Myanmar): Burman arc or Himalayan-derived?. Journal of the
687   Geological Society, 165(6), 1045-1057.
688   Adas, M.: The Burma Delta: Economic Development and Social Change on an Asian
689   Rice Frontier, 1852–1941, New Perspectives in SE Asian Studies, Univ of Wisconsin
690   Press, 276 pp., 2011.
691   Bender, F., 1983. Geology of Burma, 293 p. Gebrüder Borntraeger, Berlin.
692   Brakenridge, G. R., Syvitski, J. P. M., Nieburh, E., Overeem, I., Higgins, S. A., Kettner,
693   A. J. and Prades, L., 2017, Design with nature: causation and avoidance of
694   catastrophic flooding, Myanmar. Earth-Science Rev. 165, 81–109,.
695   British Admiralty: Bay of Bengal. East Coast. Sheet III. Coronge Island to White Point,
696   including the Gulf of Martaban, 1935.
697   Bronk Ramsey, C.: Bayesian analysis of radiocarbon dates. Radiocarbon, 51(1), 337-360,
698   2009.
699   Chhibber H. L., 1934, The Geology of Burma. Macmillan, London, 538 pp
700   Colarossi, D., Duller, G. A. T., Roberts, H. M., Tooth, S. & Lyons, R. 2015: Comparison
701   of paired quartz OSL and feldspar post-IR IRSL dose distributions in poorly bleached
702   fluvial sediments from South Africa. Quaternary Geochronology 30, 233-238.
703   Colin, C., Turpin, L., Bertraux, J., Desprairies, A. & Kissel, C. 1999. Erosional history of
704   the Himalayan and Burman ranges during the last two glacial–interglacial cycles.
705   Earth and Planetary Science Letters, 171, 647–660
706   Croudace, I. W. and Rothwell, R. G.: Micro-XRF Studies of Sediment Cores,
707   Developments in Paleoenvironmental Research, 17, Springer, 656 pp., 2015.
708   Croudace, I. W., Rindby, A. and Rothwell, R. G. ITRAX: description and evaluation of a
709   new X-ray core scanner. In New Techniques in Sediment Core Analysis (ed.
710   Rothwell, R. G.) Geol. Soc. Lond. Spec. Publ. 267, 51–63, 2006.
711   Cui, M, Wang, Zhanghua, Nageshwara Rao, Kakani, Sangode, S. J., Saito, Yoshiki, Ting,
712   Chen, Kulkarni Y. R., Ganga Kumar, K. Ch. V., Demudu.: A mid-to-late Holocene
713   record of vegetation decline and erosion triggered by monsoon weakening and human
714   adaptations in the south–east Indian Peninsula; The Holocene, 0959683617715694,
715   2017.
716   Curray, J. R., Moore, D. G., Lawver, L.A., Emmel, F.J., and Raitt, R.W.: Tectonics of the
717   Andaman Sea and Myanmar, in Watkins, J., et al., eds., Geological and Geophysical
718   Investigations of Continental Margins: American Association of Petroleum
719   Geologists Memoir 29, 189–198, 1979.
720   Curray, J. R.: Tectonics of the Andaman Sea region: Journal of Asian Earth Sciences, v.
721   25, 187–232, doi: 10.1016 /j.jseaes .2004 .09 .001, 2005.
722   D'Arrigo, R. and Ummenhofer, C. C.: The climate of Myanmar: evidence for effects of
723   the Pacific Decadal Oscillation, Int. J. Climatol., 35, 634–640, doi:10.1002/joc.3995,
724   2014.
725   Damodararao K., Singh S. K, Rai V. K., Ramaswamy, V. and Rao, P. S.: Lithology,
726   Monsoon and Sea-Surface Current Control on Provenance, Dispersal and Deposition
727   of Sediments over the Andaman Continental Shelf. Front. Mar.Sci.3:118, 2016.

728 Darby, S. E., Hackney, C. R., Leyland, J., Kummu, M., Lauri, H., Parsons, D. R., Best, J.
729   L., Nicholas, A. P. and Aalto, R.: Fluvial sediment supply to a mega-delta reduced by
730   shifting tropical-cyclone activity, Nature 539, (7628), 276-279, 2016.
731 Dixit, Y., Hodell, D. A., and Petrie, C. A., 2014, Abrupt weakening of the summer
732   monsoon in northwest India ~4100 yr ago: Geology. doi:10.1130/G35236.1.
733 Duller, G. A. T. 2003: Distinguishing quartz and feldspar in single grain luminescence
734   measurements. Radiation Measurements 37, 161–165.
735 Farr, T. G., Rosen, P. A., Caro, E., Crippen, R., Duren, R., Hensley, S., Kobrick, M.,
736   Paller, M., Rodriguez, E., Roth, L. and Seal, D.: The Shuttle Radar Topography
737   Mission. Rev Geophys 45: 10.1029/2005RG000183, 2007.
738 Fritz, H. M., Blount, C. D., Thwin, S., Thu, M. K. and Chan, N.: Cyclone Nargis storm
739   surge in Myanmar. Nature Geoscience, 2, 448-449, 2009.
740 Furuichi, T., Win, Z., Wasson, R.J.: Discharge and suspended sediment transport in the
741   Ayeyarwady River, Myanmar: centennial and decadal changes. Hydrol. Process. 23
742   (11), 1631–1641, 2009.
743 Garzanti, E., Wang, J. G., Vezzoli, G. and Limonta, M.: Tracing provenance and
744   sediment fluxes in the Irrawaddy River basin (Myanmar). Chemical Geology, 440,
745   73–90, 2016.
746 Gebregiorgis, D., Hathorne, E. C., Sijinkumar, A. V., Nagender Nath, B., Nürnberg, D.
747   and Frank, M.: South Asian summer monsoon variability during the last ~54 kyrs
748   inferred from surface water salinity and river run off proxies, Quaternary Science
749   Reviews 138: 6-15, 2016.
750 Giosan, L., Constantinescu, S., Clift, P. D., Tabrez, A. R., Danish, M. and Inam, A.:
751   Recent morphodynamics of the Indus delta shore and shelf. Continental Shelf
752   Research, 26(14),1668-1684, 2006.
753 Giosan, L., Ponton, C., Usman, M., Blusztajn, J., Fuller, D., Galy, V., Haghipour, N.,
754   Johnson, J., McIntyre, C., Wacker, L. and Eglinton, T.: Massive Erosion in
755   Monsoonal Central India Linked to Late Holocene Landcover Degradation, Earth
756   Surface Dynamics, in review, 2017.
757 Giosan, L., Syvitski, J. P. M., Constantinescu, S., Day, J.: Protect the World's Deltas,
758   Nature, 516: 31-33, 2014.
759 Godfrey-Smith, D. L., Huntley, D. J. & Chen, W. H., 1988: Optically dating studies of
760   quartz and feldspar sediment extracts. Quaternary Science Reviews 7, 373–380.
761 Goodbred S. L. and Saito, Y.: Tide dominated deltas. In Principles of Tidal
762   Sedimentology, ed. RA Davis Jr, RW Dalrymple, pp. 129–49. London: Springer,
763   2012.
764 Gordon, R.: Hydraulic work in the Irawadi Delta. Proc. Inst. Civ. Eng. 113 (1893), 276–
765   313, 1893.
766 Hedley, P. J., Bird, M. I. and Robinson, R. A. J.: Evolution of the Irrawaddy delta region
767   since 1850. Geogr. J. 176 (2), 138–149, 2010.
768 Hoitink, A. J. F., Wang, Z. B., Vermeulen, B., Huismans, Y. and Kästner, K.: Tidal
769   controls on river delta morphology. Nature Geoscience, 10(9), 637-645, 2017.
770 Kars, R. H., Reimann, T., Ankjaergaard, C. & Wallinga, J. 2014: Bleaching of the post-
771   IR IRSL signal: new insights for feldspar luminescence dating. Boreas 43, 780–791.

772 Kravtsova, V. I., Mikhailov, V. N. and Kidyaeva, V. M.: Hydrological regime,
773   morphological features and natural territorial complexes of the Irrawaddy River Delta
774   (Myanmar). Vodn. Resur. 36, 259–276, 2009.
775 Lee, H.Y., Chung, S.L. and Yang, H.M., 2016, Late Cenozoic volcanism in central
776   Myanmar: Geochemical characteristics and geodynamic significance, Lithos 245,
777   174-190
778 Liang, M., Kim, W. and Passalacqua, P.: How much subsidence is enough to change the
779   morphology of river deltas?. Geophysical Research Letters, 43(19), 2016.
780 Licht, A., Reisberg, L., France‑Lanord, C., Naing Soe, A., & Jaeger, J. J. (2016).
781   Cenozoic evolution of the central Myanmar drainage system: insights from sediment
782   provenance in the Minbu Sub‑Basin. Basin Research, 28(2), 237-251.
783 Liu, C. Z., Chung, S. L., Wu, F. Y., Zhang, C., Xu, Y., Wang, J. G., ... & Guo, S. (2016).
784   Tethyan suturing in Southeast Asia: Zircon U-Pb and Hf-O isotopic constraints from
785   Myanmar ophiolites. Geology, 44(4), 311-314.
786 Madsen, A.T., Buylaert, J.-P. & Murray, A.S. 2011. Luminescence dating of young
787   coastal deposits from New Zealand using feldspar. Geochronometria 38, 378-390.
788 Matamin, A. R., Ahmad, F., Mamat, M., Abdullah, K. and Harun, S.: Remote sensing of
789   suspended sediment over Gulf of Martaban. Ekologia, 34(1), 54-64, 2015.
790 McHugh, M. G. C., Gurung, D., Giosan, L., Ryan, W.B.F., Mart, Y., Sancar, U., Burckle,
791   L., Çagatay, M. N.: The last reconnection of the Marmara Sea (Turkey) to the World
792   Ocean: A paleoceanographic and paleoclimatic perspective, Marine Geology, 255,
793   2008.
794 Milliman, J. D. and Farnsworth, K. L.: River Discharge to the Coastal Ocean: A Global
795   Synthesis. Cambridge Univ. Press, Cambridge, 2010.
796 Moore E. H.:, Early Landscapes of Myanmar, River Books, Bangkok , pp., 272, 2007.
797 Morley, C.K. 2017. Cenozoic rifting, passive margin development and strike-slip faulting
798   in the Andaman Sea: a discussion of established v. new tectonic models. In:
799   Bandopadhyay, P.C. & Carter, A. (eds) The Andaman–Nicobar Accretionary Ridge:
800   Geology, Tectonics and Hazards. Geological Society, London, Memoirs, 47, 27–50,
801   https://doi.org/10.1144/M47.4
802 Murray, A. S. & Wintle, A. G. 2000: Luminescence dating of quartz using an improved
803   single-aliquot regenerative-dose protocol. Radiation Measurement 32, 57–73
804 Murray, A. S., Marten, R., Johnston, A. & Martin, P. 1987: Analysis for naturally
805   occurring radionuclides at environmental concentrations by gamma spectrometry.
806   Journal of Radioanalytical and Nuclear Chemistry 115, 263–288.
807 Murray, A. S., Thomsen, K. J., Masuda, N., Buylaert, J.-P. & Jain, M. 2012: Identifying
808   well-bleached quartz using the different bleaching rates of quartz and feldspar
809   luminescence signals. Radiation Measurements 47, 688–695.
810 Ota, Y., Kawahata, H., Murayama, M., Inoue, M., Yokoyama, Y., Miyairi, Y., Aung, T.,
811   Hossain, H. M. Z., Suzuki, A., Kitamura, A., Moe, K. T.: Effects of intensification of
812   the Indian Summer Monsoon on northern Andaman Sea sediments during the past
813   700 years. J. Quat. Sci. 32, 528–539, 2017.
814 Ponton, C., Giosan, L., Eglinton, T. I., Fuller, D. J., Johnson, E., Kumar, P. and Collet, T.
815   S.: Holocene Aridification of India. Geophysical Research Letters, 39, p. L03704,
816   2012.

817 Racey, A. and Ridd, M.F.: Petroleum Geology of Myanmar. Geological Society of
818   London, 2015.
819 Ramaswamy V., Rao P. S., Rao K. H., Thwin, S., Rao, Srinivasa N. and Raiker, V.: Tidal
820   influence on suspended sediment distribution and dispersal in the northern Andaman
821   Sea and Gulf of Martaban Marine Geology 208 33–42, 2004.
822 Ramaswamy, V., and Rao, P. S.The Myanmar continental shelf. In F. L. Chiocci & A. R.
823   Chivas (Eds.), Continental Shelves of the World: Their Evolution During the Last
824   Glacio-Eustatic Cycle (pp. 231-240). Bath, UK: Geological Society of London, 2014.
825 Rao, P. S., Ramaswamy, V. and Thwin, S.: Sediment texture, distribution and transport
826   on the Ayeyarwady continental shelf, Andaman Sea. Mar. Geol. 216, 239–247 2005.
827 Reimer P. J., Bard, E., Bayliss, A., Beck, J. W., Blackwell, P. G., Bronk, Ramsey C,
828   Buck, C. E., Edwards, R. L., Friedrich, M., Grootes, P. M., Guilderson, T. P.,
829   Haflidason, H., Hajdas, I., Hatté, C., Heaton, T. J., Hoffman, D. L., Hogg, A. G.,
830   Hughen, K. A., Kaiser, K. F., Kromer, B., Manning, S. W., Niu, M., Reimer, R. W.,
831   Richards, D. A., Scott, M., Southon, J. R., Staff, R. A., Turney, C. S. M., van der
832   Plicht, J.: IntCal13 and Marine13 radiocarbon age calibration curves 0–50,000 years
833   cal BP. Radiocarbon 55(2): 1869-1887, 2013.
834 Rémillard, A.M., St-Onge, G., Bernatchez, P., Hétu, B., Buylaert, J.-P., Murray, A.S.,
835   Vigneault, B., 2016. Chronology and stratigraphy of the Magdalen Islands
836   archipelago from the last glaciation to the early Holocene: new insights into the
837   glacial and sea-level history of eastern Canada. Boreas, 45, 604-628.
838 Rizal, S., Damm, P., Wahid, M.A., Sundermann, J., Ilhamsyah, Y. and Iskandar T.:
839   General circulation in the Malacca Strait and Andaman Sea: A numerical model
840   study. American Journal of Environmental Sciences. 8. 479-488.
841   10.3844/ajessp.2012.479.488. , 2012.
842 Robinson, R. A. J., Bird, M. I., Oo, N. W., Hoey, T. B., Aye, M.M., Higgitt, D. L., Swe,
843   A., Tun, T. and Win, S.L.: The Irrawaddy river sediment flux to the Indian Ocean: the
844   original nineteenth-century data revisited. The Journal of Geology, 115(6), 629-640,
845   2007.
846 Rodolfo, K. S., 1969a, Bathymetry and marine geology of the Andaman Basin, and
847   tectonic implications for Southeast Asia Geological Society of America Bulletin 80:
848   1203–1230
849 Rodolfo, K. S., 1969b, Sediments of the Andaman Basin, Northeastern Indian Ocean.
850   Mar. Geol. 7, 371– 402.
851 Rodolfo, K.S., 1975. The Irrawaddy Delta: Tertiary setting and modern offshore
852   sedimentation. In Deltas: Models for Exploration, Broussard ML (ed.). Houston
853   Geological Society: Houston; 329–348.
854 Scher H. D. and M. L.: Delaney, Braking the glass ceiling for high resolution Nd records
855   in early Cenozoic paleoceanography, Chemical Geology 269, 269-329, 2010..
856 Seekins, D. M.: "State, society and natural disaster: cyclone Nargis in Myanmar
857   (Burma)", Asian Journal of Social Science, 37(05), pp.717-37, 2009.
858 Shi, W. and Wang, M.: Three-dimensional observations from MODIS and CALIPSO for
859   ocean responses to cyclone Nargis in the Gulf of Martaban. Geophysical Research
860   Letters, 35, L21603, 2008.
861 Stamp, D. L. The Irrawaddy River. Geogr. J. 5, 329–352, (1940).

862 Swift, D. J. P. and Thorne, J. A.: Sedimentation on Continental Margins, I: A General
863   Model for Shelf Sedimentation, in Shelf Sand and Sandstone Bodies: Geometry,
864   Facies and Sequence Stratigraphy (eds D. J. P. Swift, G. F. Oertel, R. W. Tillman and
865   J. A. Thorne), Blackwell Publishing Ltd., Oxford, UK. doi:
866   10.1002/9781444303933.ch1, 1992.
867 Syvitski, J. P., Kettner, A. J., Overeem, I., Hutton, E.W., Hannon, M.T., Brakenridge,
868   G.R., Day, J., Vörösmarty, C., Saito, Y., Giosan, L. and Nicholls, R.J., Sinking deltas
869   due to human activities. Nature Geoscience, 2(10), 681-686, 2009.
870 Ta, T. K. O., Nguyen, V. L., Tateishi, M., Kobayashi, I., Saito, Y. and Nakamura, T.,
871   Sediment facies and Late Holocene progradation of the Mekong River Delta in Bentre
872   Province, southern Vietnam: an example of evolution from a tide-dominated to a tide-
873   and wave-dominated delta. Sedimentary Geology, 152(3), 313-325, 2002.
874 Taft, L. and Evers, M.: A review of current and possible future human-water dynamics in
875   Myanmar's river basins. Hydrological Earth System Science 20: 4913-4928, 2016.
876 Tanabe, S., Hori, K., Saito, Y., Haruyama, S. and Kitamura, A.: Song Hong (Red River)
877   delta evolution related to millennium-scale Holocene sea-level changes. Quaternary
878   Science Reviews, 22(21), 2345-2361, 2003.
879 Thomsen, K., Murray, A. S., Jain, M. & Bøtter-Jensen, L. 2008: Laboratory fading rates
880   of various luminescence signals from feldspar-rich sediment extracts. Radiation
881   Measurements 43, 1474–1486.
882 Van der Horst, T., 2017. Sinking Yangon: Detection of subsidence caused by
883   groundwater extraction using SAR interferometry and PSI time-series analysis for
884   Sentinel-1 data. MS Thesis, Delft University of Technology and the National
885   University of Singapore, http://repository.tudelft.nl
886 Volker, A.: The deltaic area of the Irrawaddy river in Burma in Scientific problems of the
887   humid tropical zone deltas and their implications Proceedings of the Dacca
888   Symposium UNESCO 373–9, 1966.
889 Wang, N., Li, G., Qiao, L., Shi, J., Dong, P., Xu, J. and Ma, Y.: Long-term evolution in
890   the location, propagation, and magnitude of the tidal shear front off the Yellow River
891   Mouth. Continental Shelf Research, 137, 1-12, 2017.
892
893

894   Table 1. Results of AMS ^{14}C dating of organic materials from drill cores IR1 (Kyonmangay) and IR2 (Ta Loke Htaw).
895

896

Location	Sample	Altitude (m bsl)	Type	Labcode	Latitude	Longitude	Age (years BP)	Error (years BP)	d13C (per mil)	Calibrated Age (years)*	Error (years)	Observations
Kyonmangay	IR1-9.60	-2.9	leaf fragment	OS-132754	16°26'15N	95°08'01"E	5,590	100	-28.65	6487	213	small
Kyonmangay	IR1-20.0	-13.3	leaf fragment	OS-132658	16°26'15N	95°08'01"E	7,300	40	-26.71	8166	80	
Kyonmangay	IR1-35.0	-28.3	mangrove wood piece	OS-133490	16°26'15N	95°08'01"E	8,300	40	-27.27	9352	148	
Kyonmangay	IR1-40.0	-33.3	carbonized wood piece	OS-132659	16°26'15N	95°08'01"E	9,100	35	-26.58	10351	88.5	
Ta Loke Htaw	IR2-19.0	-0.5	wood trunk piece	OS-133606	17°39'13"N	95°26'2"E	1,320	15	-28.04	1307	53.5	
Ta Loke Htaw	IR2-33.5	-15.0	carbonized wood piece	OS-135132	17°39'13"N	95°26'2"E	8,020	30	-27.7	8959	117.5	small

897   *Calendar ages are relative to year 2016
898

899 Table 2. Summary of the quartz and feldspar luminescence data. (n) denotes the number of aliquots contributing to dose (De). The
900 saturated water content (w.c.) is given as the ratio of weight of water to dry sediment weight. Feldspar IR50 and pIRIR150 ages have
901 not been corrected for any signal instability. Radionuclide concentrations used to derive quartz and feldspar dose rates are given in
902 Table S1. Bleaching of quartz OSL signal is assessed by comparing the quartz ages with the IR50 and pIRIR150 ages. Uncertainties
903 represent one standard error. Age uncertainties include random and systematic components. Quartz ages should be used for
904 interpretation; feldspar ages are only used to investigate quartz OSL bleaching.

905
906

Sample code	Site	Setting	Latitude / Longitude	Depth, cm	Quartz well-bleached?	Quartz Age, ka	$pIRIR_{150}$ Age, ka	IR_{50} Age, ka	Quartz Dose, Gy (n)	$pIRIR_{150}$ Dose, Gy	IR_{50} Dose, Gy (n)	Quartz Dose rate, Gy/ka	K-feldspar Dose rate, Gy/ka	w.c. %
17 72 01	I8	fluvial levee	N 17 38 36.82 / E 95 18 33.64	95	probably	1.50 ± 0.23	6.64 ± 0.68	1.20 ± 0.23	3.28 ± 0.49 34	20.6 ± 1.9	3.73 ± 0.69 9	2.19 ± 0.10	3.10 ± 0.12	29
17 72 02	I9	fluvial levee	N 17 36 13.5 / E 95 12 53.39	110	not certain	1.75 ± 0.32	15.2 ± 5.5	4.02 ± 1.85	4.14 ± 0.73 35	46 ± 16	12.0 ± 5.5 9	2.37 ± 0.10	2.99 ± 0.11	35
17 72 03	I10	beach ridge	N 16 09 03.5 / E 94 43 57.3	92	probably	1.46 ± 0.22	2.35 ± 0.21	1.10 ± 0.07	2.97 ± 0.42 40	6.9 ± 0.5	3.25 ± 0.17 9	2.03 ± 0.09	2.95 ± 0.11	28
17 72 04	I11	beach ridge	N 16 09.2578 / E 94 44.1843	90	confident	4.63 ± 0.47	4.73 ± 0.37	2.71 ± 0.17	10.1 ± 0.9 36	14.7 ± 1.0	8.42 ± 0.43 9	2.18 ± 0.09	3.10 ± 0.11	32
17 72 05	I12	beach ridge	N 15 50 10.5 / E 95 29 51	100	probably	1.04 ± 0.09	1.94 ± 0.19	0.79 ± 0.05	2.64 ± 0.17 38	6.7 ± 0.6	2.72 ± 0.14 9	2.53 ± 0.13	3.45 ± 0.15	38
17 72 06	I13	beach ridge	N 15 49.6494 / E 95 30.2095	132	probably	0.86 ± 0.07	1.86 ± 0.15	0.68 ± 0.04	1.58 ± 0.12 37	5.1 ± 0.4	1.88 ± 0.08 9	1.84 ± 0.07	2.75 ± 0.10	40
17 72 07	I14	beach ridge	N 16 24 27.5 / E 96 02 20.2	115	probably	1.19 ± 0.11	1.43 ± 0.12	0.76 ± 0.04	2.64 ± 0.19 40	4.5 ± 0.3	2.38 ± 0.09 9	2.21 ± 0.10	3.13 ± 0.12	24

907

908   Fig. 1. Physiography (left) and geology (right) of the Ayeyawady Basin and adjacent regions.
909
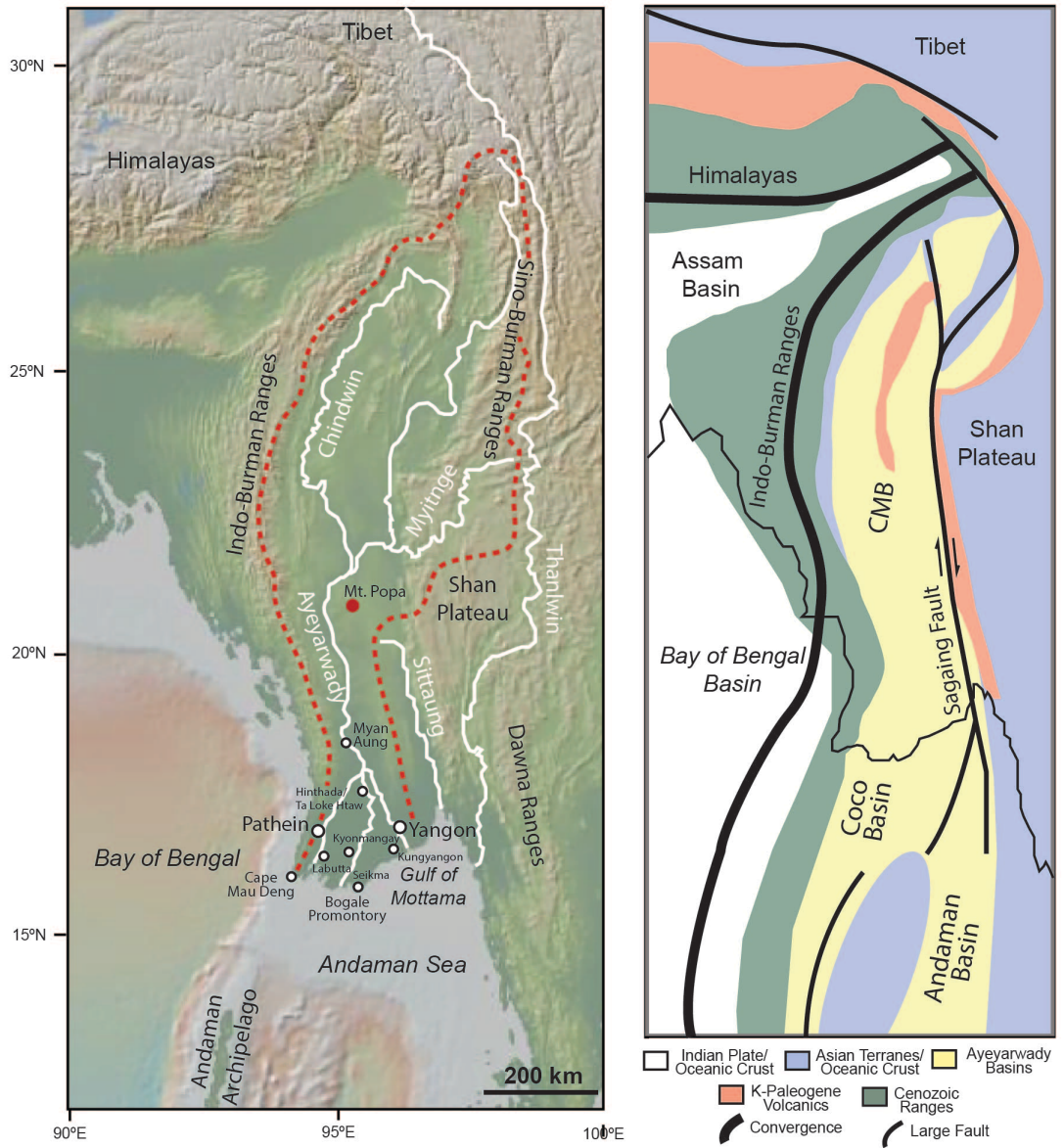
910
911
912
913
914
915

Fig. 2. (a) SRTM-derived DEM for the Ayeyawady delta region (pattern of colors repeats every 10 m to 300 m in height; higher landscape in black); (b) large scale features of the Ayeyawady delta region with identified river and distributary courses and mouths as well as beach ridges shown on an ASTER satellite photo ; (c) sample locations and chronology on the meander belts documenting the avulsion near the delta apex (meander belts as white lines delimited from ASTER and Google Earth images); (d) Preliminary model of the Ayeyawady delta evolution with sampling locations and types with chronological information on the youngest fluvial deposits and beach ridges.
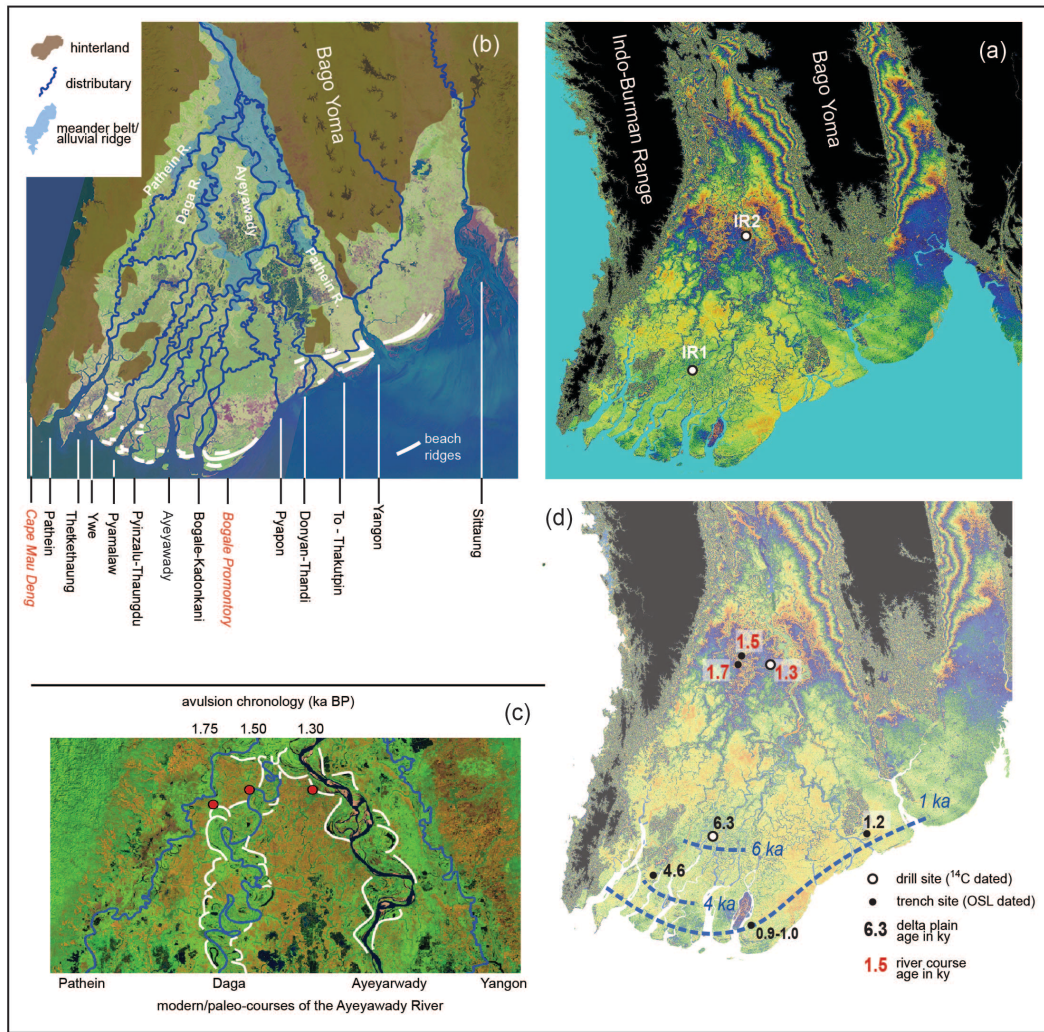
Fig. 3. (a) Depositional environments interpreted from litho- and chemo-stratigraphy with radiocarbon chronology for drill cores in the Ayeyawady delta; (b) Interpreted Ayeyawady delta stratigraphy and evolution along the Ayeyawady's main course.
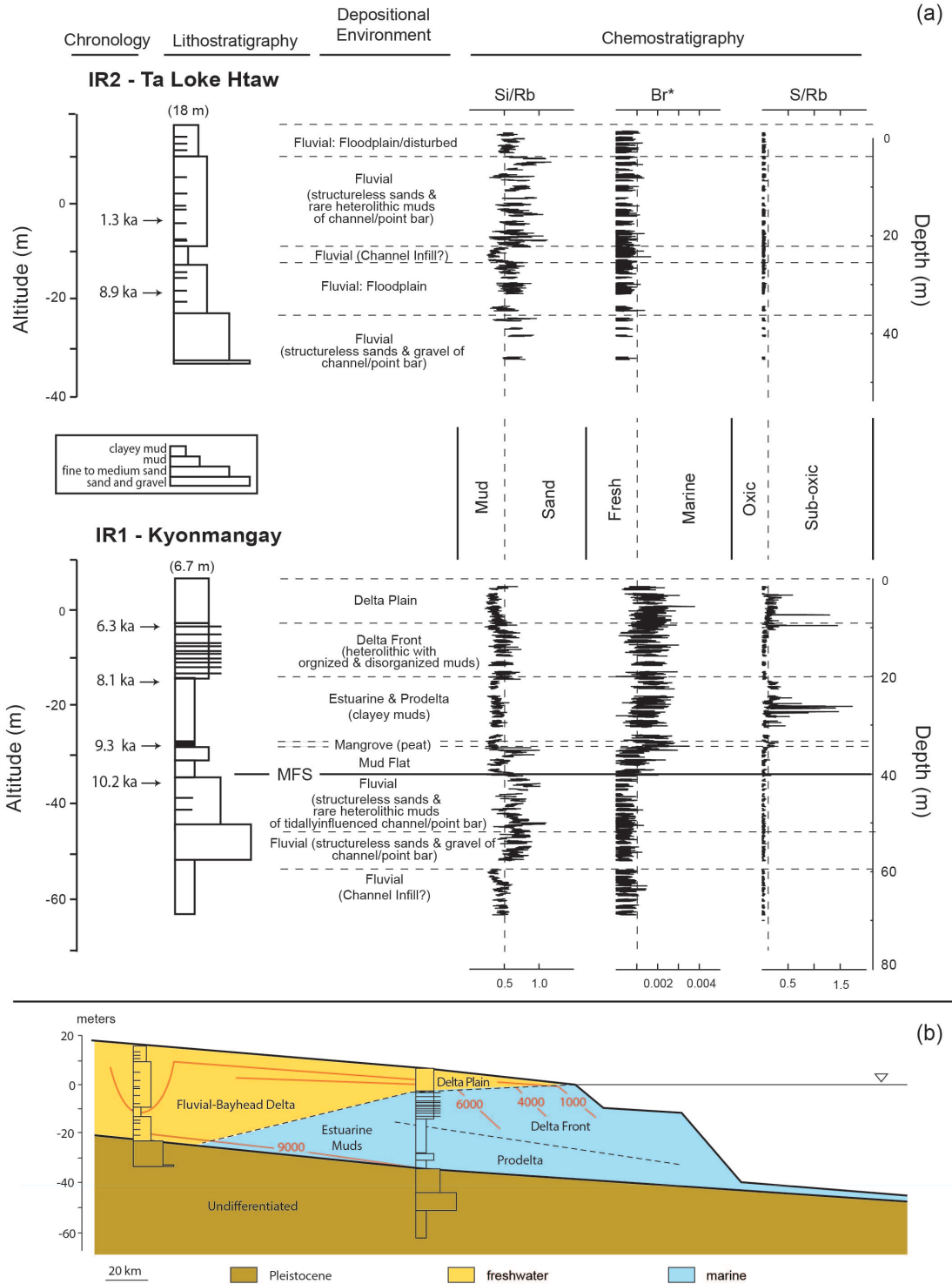
933 Fig. 4. Interpreted bathymetric profiles across the northern Andaman Sea shelf (bathymetric
934 profiles identified on map). Dashed line on map indicates the approximate limit of consistent
935 fine-grained sediment deposition on the shelf farthest from shore. The SRTM-derived DEM
936 for the Ayeyawady delta region is shown onland.
937
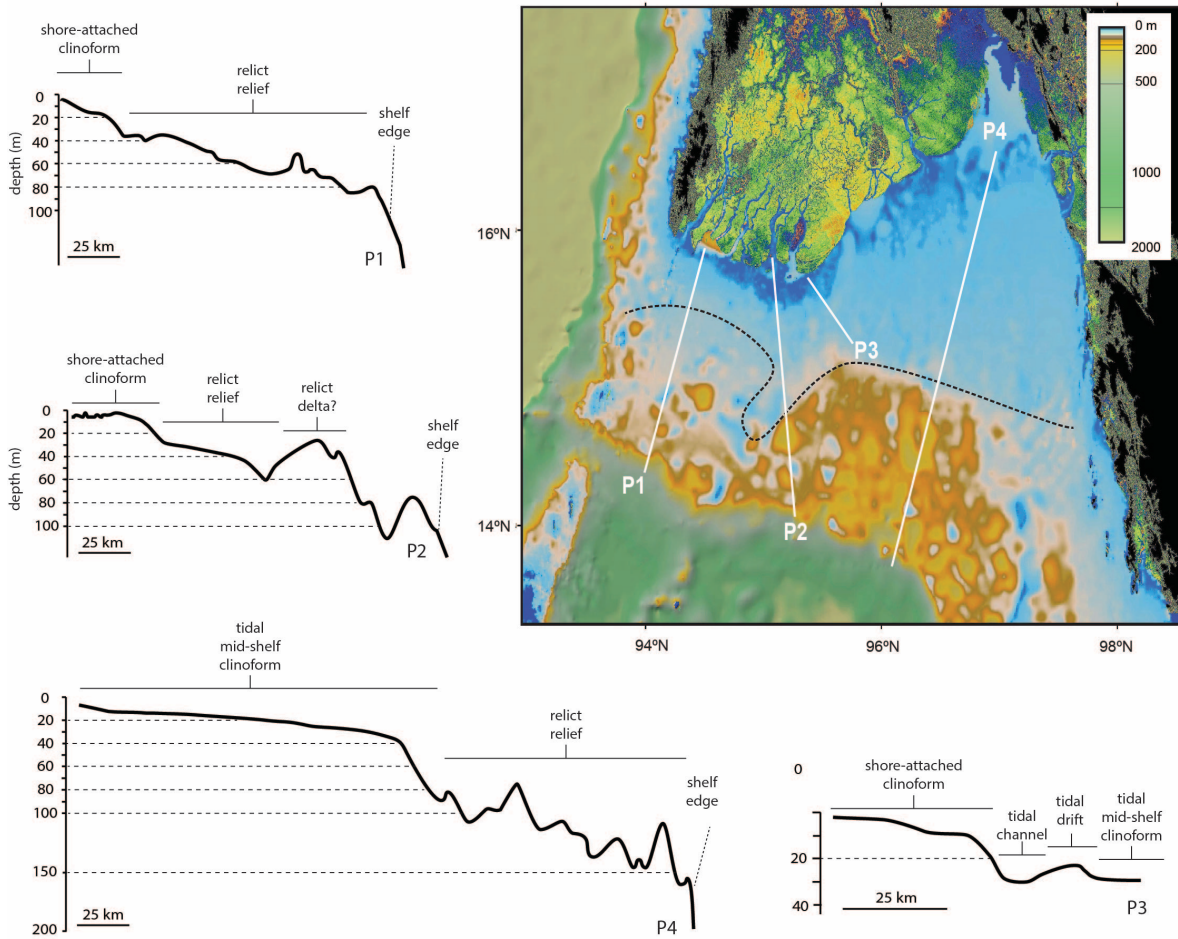
938
939
940
941
942
943
944
945
946
947
948
949
950
951
952
953
954

955 Fig. 5. (Upper) Bathymetry of the northern Andaman Sea shelf and SRTM-derived DEM for
956 the Ayeyawady delta region onland with regional faults and associated splay faults (Morley,
957 2017); arrow pairs indicate regional compression (white) or extension (red); (Middle) Tidal
958 range lines (black), co-tidal lines (white) and tidal current magnitudes (ellipses) for the
959 dominant M2 tide component (Rizal et al., 2012); (Lower) Sketch he Ayeyawady delta plain
960 evolution phases and associated subaqueous deltas.
961

962